Mn doping to enhance energy storage performance of lead-free 0.7NBT-0.3ST thin films with weak oxygen vacancies

Yulei Zhang,[1] Weili Li,[1,2,a)] Wenping Cao,[3] Yu Feng,[1] Yulong Qiao,[1] Tiandong Zhang,[1] and Weidong Fei[1,b)]

[1]*School of Materials Science and Engineering, Harbin Institute of Technology, Harbin 150001, People's Republic of China*

[2]*National Key Laboratory of Science and Technology on Precision Heat Processing of Metals, Harbin Institute of Technology, Harbin 150001, People's Republic of China*

[3]*School of Light Industry, Harbin University of Commerce, Harbin 150028, People's Republic of China*

(Received 20 March 2017; accepted 4 June 2017; published online 15 June 2017)

In this study, we present an effective strategy to enhance energy-storage density by the Mn^{2+} substitution of Ti^{4+} into $0.7(Na_{0.5}Bi_{0.5})TiO_3$-$0.3SrTiO_3$ (0.7NBT-0.3ST) relaxor ferroelectric thin films. The influence of Mn doping on the microstructures, ferroelectric properties, and energy-storage performances of the as-prepared films was investigated in detail. The results show that the values of electric break-down field strength and the difference values between maximum polarization and remnant polarization of the thin films are markedly improved by appropriate Mn doping. Owing to the high break-down field strength of 1894 kV/cm and the huge difference value between the maximum polarization and the remnant polarization of 56 μC/cm^2, a giant recoverable energy-storage density of 27 J/cm^3 was obtained for the 1 mol. % Mn-doped 0.7NBT-0.3ST thin film. These results indicate that the appropriately Mn-doped 0.7NBT-0.3ST thin films are promising for the application of advanced capacitors with high-energy storage density. *Published by AIP Publishing.*
[http://dx.doi.org/10.1063/1.4986468]

www.spm.com.cn

Dielectric materials with high energy storage density, fast charge/discharge, low cost, and good temperature stability have been extensively investigated in the past few decades and will be surely further and deeply studied in the future for the potential capability of storing electric energy and applications in advanced electronics.[1–7] Among various dielectric material capacitors, film capacitors for dielectric energy storage have attracted increasing attention due to their high break-down strength (BDS) and hence their higher power density among the energy storage devices. By far, a majority of studies on film capacitors have been focused on lead-based materials. However, lead-containing materials are considered to be a serious threat to the environment and human health. Therefore, the developments of lead-free materials with higher energy-storage density are highly required.[8–14]

In general, the energy-storage density (W) of dielectric materials could be estimated from the polarization versus electric field (P-E) curves and calculated with the following equation:

$$W = \int_{P_r}^{P_{max}} E dP, \quad (1)$$

where E is the applied electric field, P is the polarization, P_{max} is the maximum polarization, and P_r is the remnant polarization. Considering the above equation, dielectric materials possessing smaller P_r, larger P_{max}, and higher BDS should be potential candidates for high recoverable energy-storage applications.[15–20]

As typical relaxor ferroelectrics, (1–x)NBT-xST systems which exhibit slim P-E loops and diffused phase transition have attracted much attention, and it is reported that the high energy density and good temperature-dependent energy-storage stability can be obtained when the value of x is 0.3.[6,21,22] The compound of 0.7NBT-0.3ST can be considered as one of the most promising candidates to replace lead-based energy storage materials. Although progress has been made in the researches on lead-free thin films for energy storage, the performances of lead-free thin films were found to be still far inferior to those of lead-based materials. There are two possible routes to improve the energy-storage density: one is to enlarge the difference value between P_{max} and P_r. The other is to enhance the value of BDS. On the one hand, in order to improve the BDS, appropriate oxygen vacancies can be introduced to act as trap sites, thereby, electron trap levels become deeper.[23] Acceptor doping usually introduces oxygen vacancies and defect dipoles.[24–27] Defect dipoles could provide an intrinsic restoring force, thus causing a deduction in P_r. On the other hand, according to the theory of Landau-Ginsburg-Devonshire, the compressive stress can make the Gibbs free energy flat[28] and then reduce the ferroelectric domain reversal barrier, thereby increasing the P_{max}. Usually, doping large atoms at small atom sites will make the lattice constant become larger[29] and introduce compressive stress in the local area.

According to the above discussions, in this work, we present an effective strategy to enhance energy-storage density by the Mn^{2+} substitution of Ti^{4+} in 0.7NBT-0.3ST relaxor ferroelectric thin films fabricated by the Sol-Gel method. The aim is to improve the energy-storage performances of 0.7NBT-0.3ST thin films through enhancing the value of BDS and P_{max}–P_r by ion doping.

0.7NBT-0.3ST thin films doped with different contents of Mn were prepared on a Pt/Ti/SiO_2/Si substrate by the

a)Electronic mail: wlli@hit.edu.cn
b)Electronic mail: wdfei@hit.edu.cn

Sol-Gel method. Bismuth nitrate pentahydrate, sodium acetate, tetrabutyl titanate, strontium acetate, and manganese acetate were selected as the raw materials. 2-Methoxyethanol and acetic acid were used as the solvents. The concentration of the precursor solutions was adjusted to 0.2 M. After being aged for 24 h, Mn-doped 0.7NBT-0.3ST thin films were deposited on a Pt/Ti/SiO_2/Si substrate through a multiple-step spin-coating procedure. Mn-doped 0.7NBT-0.3ST wet films were spin coated at 4000 rpm for 20 s. In order to avoid the formation of cracks, every wet film was pyrolyzed on a hotplate at 350 °C for 5 min repeatedly until the desired film thickness was achieved. Finally, the films were annealed at 650 °C for 5 min, respectively, by rapid thermal annealing (RTA, the heating rate is 60 °C/s) in an oxygen atmosphere. The phase purity and crystal structure were examined by X-ray diffraction (XRD) using a Philips X'Pert diffractometer with Cu Kα radiation operating at 40 kV and 40 mA. The surface and cross-sectional morphologies of thin films were observed by atomic force microscopy (CSPM5600 of Benyuan) and scanning electron microscopy (Helios Nanolab600i), respectively. To determine the ferroelectric properties of the films, dot-type Pt electrodes with an area of 3.14×10^{-4} cm^2 were deposited on each 0.7NBT-0.3ST thin film by magnetron sputtering. Ferroelectric properties and leakage current characteristics were evaluated using a Radiant Technologies Precision workstation ferroelectric measurement system, and *P-E* loops were measured at a frequency of 1000 Hz. With the help of an Agilent 4294A precision impedance analyzer, the electric field dependence of capacitance curves of the samples was measured at an ac amplitude of 50 mV.

The crystal structure and surface and cross-sectional morphologies of thin films are shown in the supporting information. As discussed in the introduction, dielectric materials possessing smaller P_r, larger P_{max}, and high BDS should be potential candidates for high recoverable energy-storage applications. In order to obtain the full value of energy-storage density, the Weibull distribution[21] of BDS for Mn-doped 0.7NBT-0.3ST thin films is shown in Fig. 1(a). According to the data given in Fig. 1(a), the average BDS values [shown in the inset of Fig. 1(a)] are 421 kV/cm, 1894 kV/cm, 1684 kV/cm, and 842 kV/cm for 0.7NBT-0.3ST thin films doped with 0, 1, 1.3, and 1.5 mol. % Mn, respectively, indicating that Mn doping could increase the electric-field endurance of films. The current densities for pure and Mn-doped 0.7NBT-0.3ST thin films are plotted against the applied electric field and shown in Fig. 1(b). Compared with pure 0.7NBT-0.3ST thin films, the enhancement of the leakage property is realized in Mn-doped thin films. The reduction in the leakage current could improve the value of BDS in the thin films. The leakage current is the lowest when 1 mol. % Mn is doped into the film, which is consistent with the result in Fig. 1(a). In order to find out the nature of reduced leakage current in the Mn-doped 0.7NBT-0.3ST thin films, the conduction mechanism of fabricated specimens is discussed. Figures 1(c)–1(f) show the logarithmic plots of the dependence of *J* as a function of Ln*E* for fabricated specimens. The curves of all thin films can be modeled in terms of space charge-limited current (SCLC). As shown in Figs. 1(c)–1(f), in the low field region, the curves follow Ohmic conduction properties (α~1). With the increasing electric field, α changes to ~2 in agreement with the modified Child's law conduction.[30,31] When the electric field is further increased, a sharp increase in the slope (α) in the double logarithm plot occurs because of large leakage current. According to Lampert's theory of the SCLC conductions, E_c is defined as the transition electric field (Ohmic to modified

www.spm.com.cn

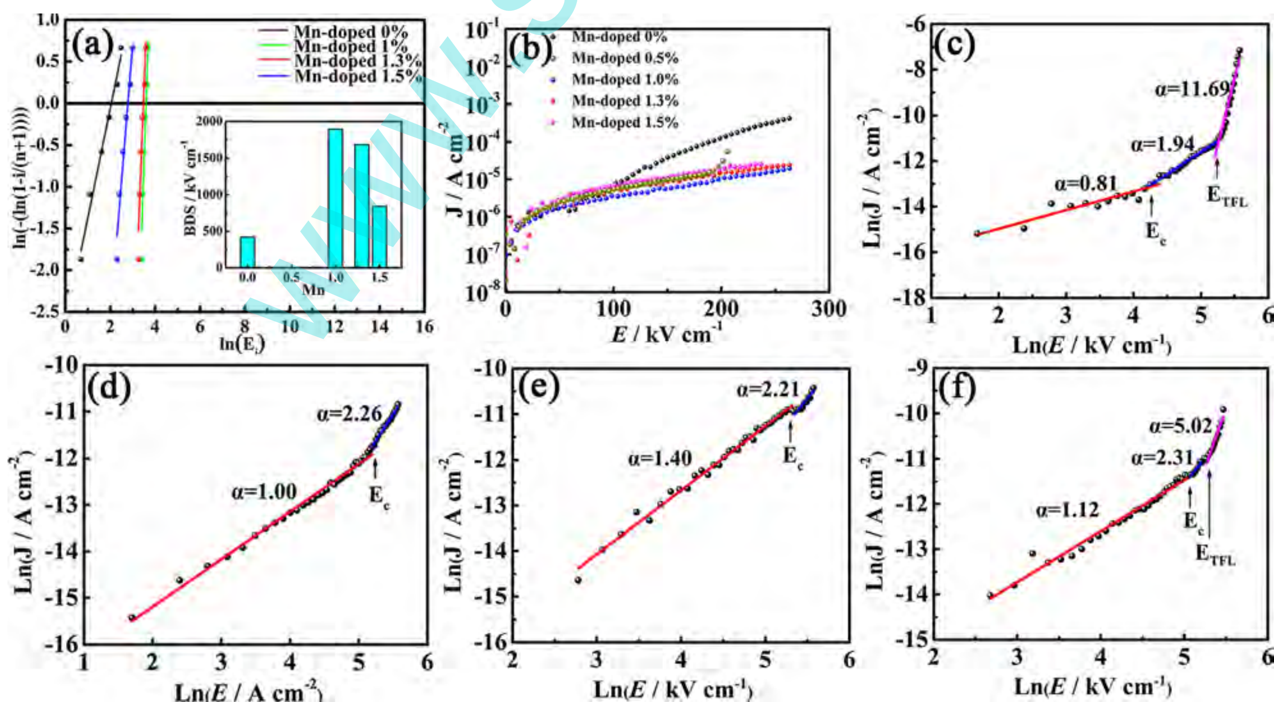

FIG. 1. (a) Weibull distributions and the fitting lines of BDS of all the samples, (b) leakage current characteristics of all samples, (c)–(f) logarithmic plots of the dependence of *J* as a function of *E* of 0.7NBT-0.3ST thin films doped with 0, 1, 1.3, and 1.5 mol. % Mn. Fits of these data are shown to help in determining the leakage mechanism.

Child's law) and E_T is defined as the transition electric field (modified Child's law to the large leakage current region). For the 1 and 1.3 mol. % Mn-doped films, E_T is not observed because the transition voltage might be higher than the scope of testing. So, the E_T for each specimen is found out as E_T(0.7NBT-0.3ST) < E_T(1.5 mol. % Mn-doped 0.7NBT-0.3ST) < E_T(1 and 1.3 mol. % Mn-doped 0.7NBT-0.3ST), which indicates that doped Mn ions in the films mainly act as carrier trap sites.[30] Also, E_c for the Mn-doped 0.7NBT-0.3ST films is much higher than that for the pure 0.7NBT-0.3ST films. Thus, this means that deep traps were formed by Mn^{2+} doping. Moreover, the greatly reduced leakage current of Mn-doped 0.7NBT-0.3ST films is closely related to such deep trap levels formed by ion doping. So, the leakage currents of Mn-doped 0.7NBT-0.3ST films in the modified Child's law conduction region have been suppressed compared to the pure 0.7NBT-0.3ST films.[30,32–34] The change in the transition electric field corresponding to the conduction mechanism may be due to electrode interface traps, grain boundary defects, and oxygen vacancies. The amount of oxygen vacancies increases with the increasing Mn doping content. When the Mn doping content exceeds 1 mol. % in the films, the probability of oxygen vacancies forming continuous paths for electron conduction is increased, resulting in a decrease in the value of BDS and an increase in leakage current. Overall, appropriate Mn^{2+} doping for the improvement of energy storage performance has a great advantage.

The polarization intensity is also a key factor affecting the energy density. Figures 2(a)–2(d) show the *P-E* hysteresis loops of Mn-doped 0.7NBT-0.3ST thin films measured from the low electric field to their critical BDS. The hysteresis loops measured at different electric fields are distinguished by different colors. It is noted that the weakly pinched *P-E* hysteresis loops can be observed when Mn is doped into thin films and Mn doping also improves the ferroelectric properties of thin films. The *P-E* curves of 1 mol. % and 1.3 mol. % Mn-doped thin films show nearly saturated polarization at their critical BDS. Due to the low leakage current, the large electric field can be applied to the film. Then, the *P-E* curves of 1% and 1.3% Mn-doped thin films show nearly saturated polarization at their critical BDS. Compared with 1 mol. % and 1.3 mol. % Mn-doped thin films, the leakage currents of 0 mol. % and 1.5 mol. % Mn-doped thin films are higher. The films are easily broken down at the weak electric field which is much smaller than the saturation field. In this case, the *P-E* curves of 0% and 1.5% Mn-doped thin films do not show nearly saturated polarization at their critical BDS. Partial rounding of *P-E* loops near the saturation field [Figs. 2(b) and 2(c)] might be caused by asymmetric electrode geometry, free carriers, and leakage. Because the area of the top electrode is much larger than the thickness of the films, the asymmetric electrode geometry has little effect on the partial rounding of *P-E* loops near the saturation field. The main reasons for this phenomenon are free carriers and leakage currents. The P_r and P_{max} values of Mn-doped 0.7NBT-0.3ST thin films measured at the same electric field are presented in Fig. 2(e). It can be clearly found that the P_r values decrease while the P_{max} values increase first and then decrease with the increasing Mn content. Figure 2(f) shows the P_{max}-P_r values of 0.7NBT-0.3ST thin films measured at their critical BDS. The maximum value of P_{max}-P_r can be up to 56 μC/cm^2 when 1 mol. % Mn is doped into the thin film.

From the above *P-E* hysteresis loops, evidently slim loops are not observed. In order to verify the presence of defect dipoles, the electric field dependence of capacitance curves is measured at 1 MHz, as shown in Fig. 3(a).The butterfly curves with a valley are observed in Mn-doped films. This demonstrates that there are defect dipoles in the films. The schematic diagram of possible mechanisms for the origin

www.spm.com.cn

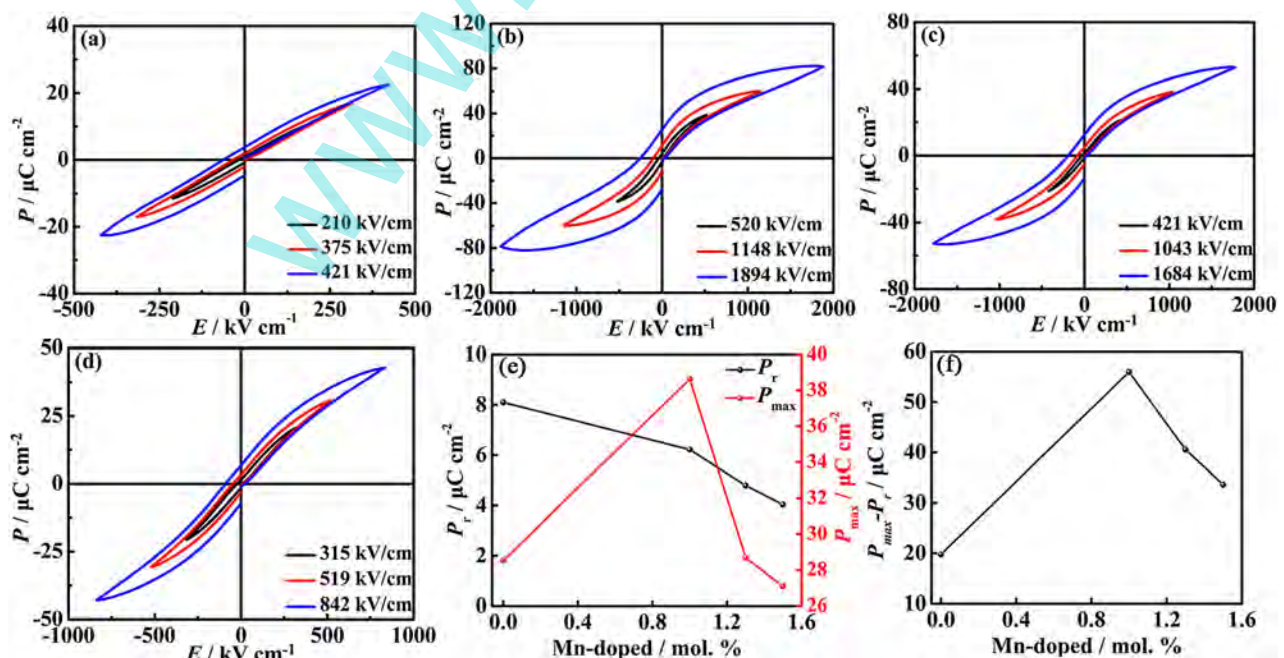

FIG. 2. (a)–(d) The *P-E* hysteresis loops of 0.7NBT-0.3ST thin films doped with 0, 1, 1.3, and 1.5 mol. % Mn measured from the low electric field to their critical BDS, (e) P_{max} and P_r values of all thin films measured at the same electric field, and (f) P_{max}-P_r values of all thin films measured at their critical BDS.

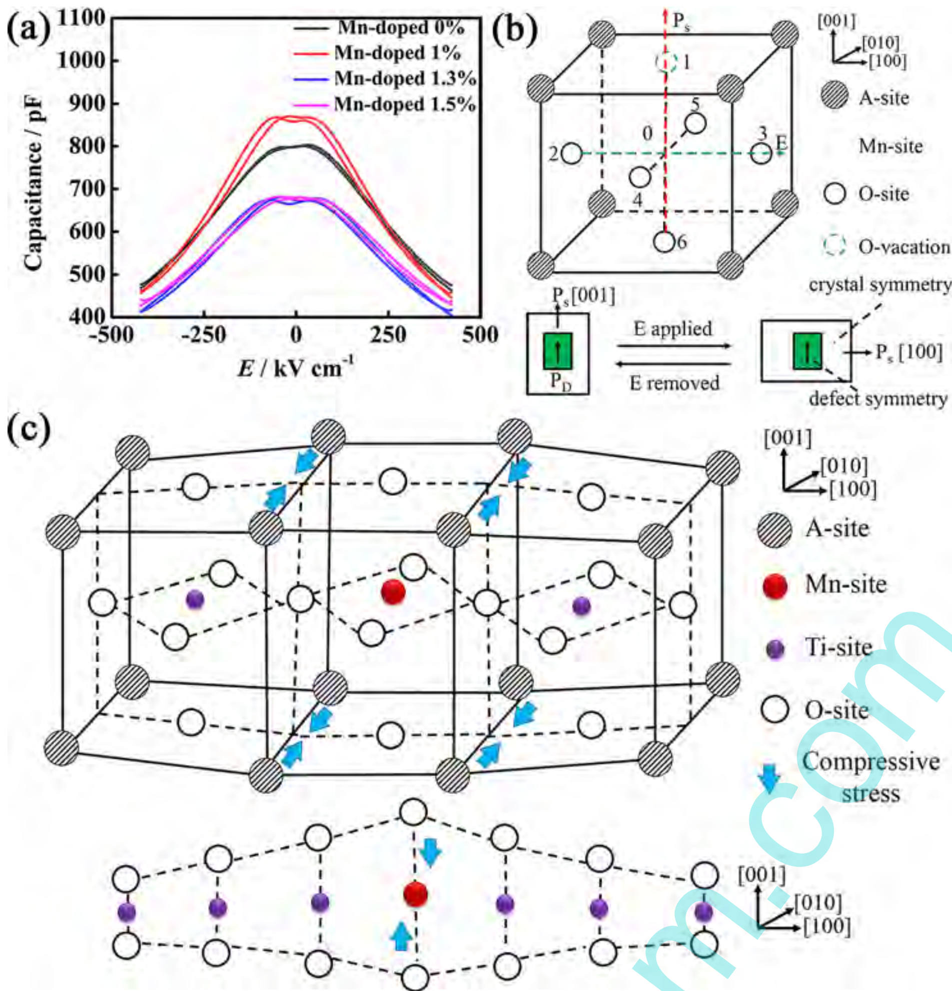

FIG. 3. (a) The electric field dependent capacitor curves of all the samples, (b) defect symmetry and tetragonal crystal symmetry in the Mn-doped tetragonal 0.7NBT-0.3ST structure, and (c) schematic illustration of compressive stress.

www.spm.com.cn

of the decrease in the P_r value induced by defect dipoles in Mn-doped thin films is depicted in Fig. 3(b). The phase structure of Mn-doped 0.7NBT-0.3ST is tetragonal.[35] It has been reported that doping acceptor Mn^{2+} at the Ti^{4+} site can create oxygen vacancies $V_O^{\bullet\bullet}$ at O^{2-} sites to maintain charge neutrality.[25–27,36] In such a case, Mn^{2+} dopants and O^{2-} vacancies act as point defects. According to the symmetry conforming property of point defects, the symmetry of short-range order distribution of point defects tends to follow the crystal symmetry when in equilibrium. Due to the Couloumb attractive force between the effectively positive O^{2-} vacancies and negative Mn^{2+} dopants, it is natural that the closer sites 1, 4, and 6 should have large defect probability. In Mn-doped thin films, the O^{2-} vacancies and Mn^{2+} can create a defect polarization P_D aligning along the spontaneous polarization (P_s) direction. When an electric field is applied to the Mn-doped sample, P_s is switched to the field E direction, but the defect symmetry and associated P_D cannot have a sudden change, as shown in the bottom illustration of Fig. 3(b). After removing the electric field, the unchanged defect symmetry and the associated P_D provide an intrinsic restoring force to switch the P_s to its original orientation so that the order of the remaining ordered domain is reduced.[25,26] Macroscopically, this reversible domain switching gives rise to a pinched *P-E* loop and a small P_r. The change trend of the P_{max} is determined from the stress. As shown in Fig. S1(b) (supplementary material), the (110) peak is shifted to a lower angle with the increasing Mn content. When the Mn doping content increases from 0 to 1.5 mol. %, the (110) diffraction peak of the film shifts 0.05° to a lower angle, which indicates that lattice constants of Mn-doped thin films increase with the increasing doping content. Because the ion radius of Mn^{2+} (0.67 Å) is larger than that of Ti^{4+} (0.61 Å), the lattice constants of Mn-doped thin films become larger.[29] Due to lattice mismatches, Mn-doped cells are subjected to compressive stress from the close-by cells [Fig. 3(c)]. It is known that compressive stress can make the Gibbs free energy flat.[28] The increase in P_{max} is a direct

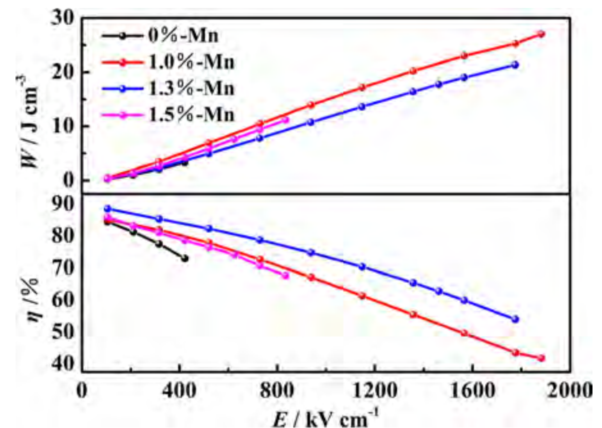

FIG. 4. The recoverable energy-storage density and energy-storage efficiency of Mn-doped 0.7NBT-0.3ST thin films.

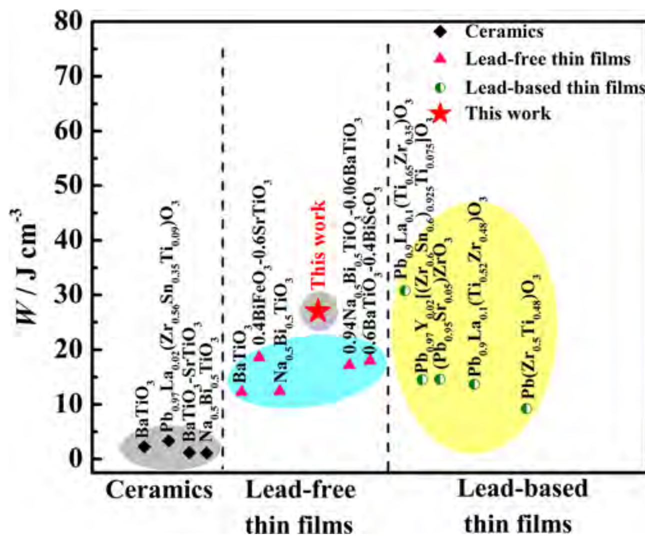

FIG. 5. Energy storage performances of representative materials.

consequence of the reduction in the ferroelectric domain reversal barrier by the anisotropic flattening of the Gibbs free energy. Excessive Mn^{2+} doping introduces a large amount of oxygen vacancies, and due to the great effect of pinning, it is difficult to switch local polarization near an oxygen vacancy, resulting in a decrease in P_{max}.[37] These changes are in line with the original design.

Figure 4 illustrates the recoverable energy-storage density W and energy-storage efficiency (η) of all samples. As is desired, with the increasing electric field, the W values of all the thin films increase. It could be easily found that the W values of Mn-doped samples have improved a lot compared to those of pure 0.7NBT-0.3ST thin films. In Mn-doped samples, 0.7NBT-0.3ST thin films doped with 1 mol. % Mn possess the highest energy storage density of about 27 J/cm^3, till now, which is higher than the previously reported values for lead-free films. For comparison, energy storage performances of representative materials are plotted, as shown in Fig. 5. According to the previous analyses, the 1 mol. % Mn-doped 0.7NBT-0.3ST thin films not only possess a large value of BDS but also high P_{max}-P_r, resulting in a high energy storage density.

In summary, lead-free Mn-doped 0.7NBT-0.3ST thin films were deposited on $Pt/Ti/SiO_2/Si$ substrates via the Sol–Gel method. Appropriate Mn doping acts as traps sites and forms deeper trap levels, and then the BDS is improved. Defect dipoles provide an intrinsic restoring force, thus causing a deduction of P_r in Mn-doped films. The compressive stress introduced by Mn^{2+} doping makes the Gibbs free energy flat and then reduces the ferroelectric domain reversal barrier, thereby increasing the P_{max}. Due to the high BDS value of 1894 kV/cm and the huge P_{max}-P_r value of 56 $\mu C/cm^2$, a giant recoverable energy density of 27 J/cm^3 was obtained for the 1 mol. % Mn-doped 0.7NBT-0.3ST thin film. These results indicate that the Mn-doped 0.7NBT-0.3ST thin films are promising for the application of advanced capacitors with high-energy storage density.

See supplementary material for the crystal structure and surface and cross-sectional morphologies of thin films.

This work was supported by the National Natural Science Foundation of China (Grant Nos. 51677033 and 51471057).

[1] Y. A. Hao and X. H. Wang, Nano Energy **31**, 49–56 (2017).
[2] B. C. Luo and X. H. Wang, J. Appl. Phys. **120**(7), 074106 (2016).
[3] M. D. Nguyen and E. P. Houwman, APL Mater. **4**(8), 080701 (2016).
[4] S. Xiao and S. M. Xiu, J. Eur. Ceram. Soc. **36**(16), 4071–4076 (2016).
[5] R. Xu and Z. Xu, Appl. Phys. Lett. **109**(3), 032903 (2016).
[6] Z. S. Xu and X. H. Hao, J. Alloys Compd. **639**, 387–392 (2015).
[7] Q. G. Chi and J. F. Dong, J. Mater. Chem. C **4**, 8179–8188 (2016).
[8] L. Yao and Z. Pan, ACS Appl. Mater. Interfaces **8**(39), 26343–26351 (2016).
[9] L. Zhang and X. H. Hao, J. Alloys Compd. **586**, 674–678 (2014).
[10] X. Zhang and Y. Shen, ACS Appl. Mater. Interfaces **8**, 27236–27242 (2016).
[11] Y. Zhao and H. C. Gao, Mater. Res. Bull. **84**, 177–184 (2016).
[12] Y. Zhao and X. H. Hao, J. Alloys Compd. **601**, 112–115 (2014).
[13] H. Y. Zheng and Y. P. Pu, J. Alloys Compd. **674**, 272–276 (2016).
[14] H. F. Zhu and M. L. Liu, Acta Mater. **122**, 252–258 (2017).
[15] Q. Li, L. Chen, M. R. Gadinski, S. Zhang, G. Zhang, H. U. Li, E. Iagodkine, A. Haque, L.-Q. Chen, T. N. Jackson, and Q. Wang, Nature **523**, 576–579 (2015).
[16] Q. Li and K. Han, Adv. Mater. **26**, 6244–6249 (2014).
[17] B. Peng, Q. Zhang, X. Li, T. Sun, H. Fan, S. Ke, M. Ye, Y. Wang, W. Lu, H. Niu, X. Zeng, and H. Huang, ACS Appl. Mater. Interfaces **7**, 13512–13517 (2015).
[18] Z. K. Xie and Z. X. Yue, Appl. Phys. Lett. **106**, 202901 (2015).
[19] M. H. Park, H. J. Kim, Y. J. Kim, T. Moon, K. D. Kim, and C. S. Hwang, Adv. Energy Mater. **4**, 1400610 (2014).
[20] Z. Yao, Z. Song, H. Hao, Z. Yu, M. Cao, S. Zhang, M. T. Lanagan, and H. Liu, Adv Mater. **29**, 1601727 (2017).
[21] W. P. Cao and W. L. Li, J. Eur. Ceram. Soc. **36**, 593–600 (2016).
[22] Y. L. Zhang and W. L. Li, Ceram. Int. **42**, 14788–14792 (2016).
[23] J. J. Huang and Y. Zhang, Appl. Phys. Lett. **96**, 042902 (2010).
[24] R. Waser and M. Klee, Integr. Ferroelectr. **2**, 23–40 (1992).
[25] L. X. Zhang and X. B. Ren, Phys. Rev. B **73**, 094121 (2006).
[26] Z. Y. Feng and X. B. Ren, Phys. Rev. B **77**, 134115 (2008).
[27] W. P. Cao and W. L. Li, Appl. Phys. Lett. **108**, 202902 (2016).
[28] M. Budimir, D. Damjanovic, and N. Setter, Phys Rev B. **72**, 064107 (2005).
[29] Y. Y. Wu, J. Am. Ceram. Soc. **94**, 3877–3882 (2011).
[30] T. Kawae, Appl. Phys. Lett. **94**(11), 112904 (2009).
[31] M. A. Lampert, Phys. Rev. **103**, 1648–1656 (1956).
[32] M. Abazari and A. Safari, Appl. Phys. Lett. **97**(26), 262902 (2010).
[33] G. W. Pabst and L. W. Martin, Appl. Phys. Lett. **90**(7), 072902 (2007).
[34] Y. Kizaki and Y. Noguchi, Appl. Phys. Lett. **89**(14), 142910 (2006).
[35] Z. Xu, X. Hao, and S. An, J. Mater. Sci.: Mater. Electron. **26**, 4318–4324 (2015).
[36] Y. Y. Liu, J. Appl. Phys. **114**, 174102 (2013).
[37] L. X. He, Phys. Rev. B **68**, 134103 (2003).

www.spm.com.cn